Copper ion incorporation in α-synuclein amyloids

Received: 18 October 2023 | Revised: 1 February 2024 | Accepted: 19 February 2024

DOI: 10.1002/pro.4956

RESEARCH ARTICLE

THE PROTEIN SOCIETY WILEY

Copper ion incorporation in α-synuclein amyloids

Gulshan Walke | **Ranjeet Kumar** | **Pernilla Wittung-Stafshede**

Department of Life Sciences, Chalmers University of Technology, Gothenburg, Sweden

Correspondence
Pernilla Wittung-Stafshede, Department of Life Sciences, Chalmers University of Technology, 412 96 Gothenburg, Sweden.
Email: pernilla.wittung@chalmers.se

Funding information
Vetenskapsrådet; Knut och Alice Wallenbergs Stiftelse

Review Editor: Jean Baum.

Abstract

Copper ion dys-homeostasis is linked to neurodegenerative diseases involving amyloid formation. Even if many amyloidogenic proteins can bind copper ions as monomers, little is known about copper interactions with the resulting amyloid fibers. Here, we investigate copper interactions with α-synuclein, the amyloid-forming protein in Parkinson's disease. Copper (Cu(II)) binds tightly to monomeric α-synuclein in vitro involving the N-terminal amine and the side chain of His50. Using purified protein and biophysical methods in vitro, we reveal that copper ions are readily incorporated into the formed amyloid fibers when present at the start of aggregation reactions, and the metal ions also bind if added to pre-formed amyloids. Efficient incorporation is observed for α-synuclein variants with perturbation of either one of the high-affinity monomer copper-binding residues (i.e., N-terminus or His50) whereas a variant with both N-terminal acetylation and His50 substituted with Ala does not incorporate any copper into the amyloids. Both the morphology of the resulting α-synuclein amyloids (amyloid fiber pitch, secondary structure, proteinase sensitivity) and the copper chemical properties (redox activity, chemical potential) are altered when copper is incorporated into amyloids. We speculate that copper chelation by α-synuclein amyloids contributes to the observed copper dys-homeostasis (e.g., reduced bioavailable levels) in Parkinson's disease patients. At the same time, amyloid-copper interactions may be protective to neuronal cells as they will shield aberrantly free copper ions from promotion of toxic reactive oxygen species.

KEYWORDS

aggregation, alpha-synuclein, amyloid, copper, reactive oxygen species

1 | INTRODUCTION

Assembly of the protein α-synuclein (aS) into β-sheet-rich amyloid fibers is linked to the molecular pathology of Parkinson's disease (PD), the second most common neurodegenerative disorder after Alzheimer's disease (Winner et al., 2011; Galvin et al., 1999). aS amyloids constitute the major content of pathological neuronal inclusions, Lewy bodies, found post-mortem in the *substantia nigra* region of PD patients (Goldberg & Lansbury, 2000; Spillantini et al., 1997; Uversky, 2007). At physiological conditions, the 140-residue aS can be detected in both an

intrinsically unstructured form in the cytosol and a helical state on lipid membranes (Lee et al., 2002; Miraglia et al., 2018). The function of aS remains obscure, but appears related to synaptic vesicle trafficking, clustering and membrane fusion (Fusco et al., 2016; Dev et al., 2003; Lassen et al., 2016). Association of aS monomers into amyloid fibers with a cross-β-structure is thought to result in toxic gain-of-functions, in similarity to other neurodegenerative diseases involving amyloid formation. The aS amyloid fibers may also transfer from one cell to another, reminiscent of prion-like spreading (Luk et al., 2012; Masuda-Suzukake et al., 2013; Recasens et al., 2014).

Studies have suggested that metal ions play pivotal roles in PD and other neurodegenerative disorders (Bush, 2000; Bjorklund et al., 2019; Aaseth et al., 2018; Bisaglia & Bubacco, 2020). Occupational long-term exposure to copper (and other heavy metals) has been associated with enhanced risk of developing PD (Bisaglia & Bubacco, 2020). In fact, imbalances of metal levels are strongly associated with many neurodegenerative diseases (Fink, 2006) and amyloid deposits in brains have been found to be enriched in metal ions (Miller et al., 2006; Lovell et al., 1998). The copper level in amyloid plaque from Alzheimer's patients was found to be near millimolar (Bush, 2003; Cheignon et al., 2018). Copper ions (Cu), as well as other metal ions, are present at higher concentrations in the brain (Gaier et al., 2013) than in other tissues, and a gradual increase in brain metal ion content is thought to be a consequence of normal aging (Valiente-Gabioud et al., 2012). In PD, Cu levels are found to be decreased in the *substantia nigra* but increased in cerebrospinal fluid and blood (Bush, 2000; Bisaglia & Bubacco, 2020).

By cycling between reduced Cu(I) and oxidized Cu(II) states, Cu provides activity to several essential enzymes in humans (Gray, 2003). In addition to being a key cofactor in enzymes, emerging data show that Cu ions also participate in cell–cell signaling at synapses (Gaier et al., 2013; D'Ambrosi & Rossi, 2015). Cu released in the synaptic cleft can transiently reach concentrations over 100 μM and such ions are thought to be in the Cu(II) form. If Cu-loaded vesicles are disrupted before fusion with the plasma membrane, Cu(II) ions could be released in the otherwise-reducing intracellular environment. In addition, because oxidative stress—that may generate damaging reactive oxygen species (ROS)—is another hallmark of PD, intracellular Cu(I) ions may become oxidized in disturbed brain cells. Thus, it is of pathological relevance that aS is annotated in UniProt (www.uniprot.org) as Cu-binding, and Cu(II) accelerate aS amyloid formation in vitro (Uversky et al., 2001; Villar-Pique et al., 2016; Moriarty et al., 2014; Binolfi et al., 2010; Wittung-Stafshede, 2022).

Both Cu(I) and Cu(II) binds to aS monomers in vitro (Camponeschi et al., 2013; de Ricco et al., 2015) and structural features, binding sites, and affinities for these interactions have been the focus of many spectroscopic studies (Camponeschi et al., 2013; de Ricco et al., 2015; Binolfi et al., 2006; Binolfi et al., 2011; Carboni & Lingor, 2015). The high affinity Cu(II) site(s) in the monomer when in solution is found in the N-terminal part and involves the N-terminal free amine, backbone atoms from Asp2 and the imidazole nitrogen of His50 (Moriarty et al., 2014; Miotto et al., 2015) (Figure 1). Mutation of His50 only somewhat reduces Cu(II) affinity (Dudzik et al., 2011; Teng et al., 2021), and the Cu(II) acceleration effect on aggregation kinetics in vitro remains (Villar-Pique et al., 2016; Mason et al., 2016). Notably, in vivo, aS is N-terminally acetylated to a large degree (Moriarty et al., 2014; Teng et al., 2021; Öhrfelt et al., 2011). This post-translational modification reduces Cu(II) affinity more dramatically than mutation of His50 (Teng et al., 2021) and, in accord, Cu(II) does not accelerate aggregation of the acetylated protein in vitro (Lorentzon et al., 2020). Whereas the Cu(II) affinity (K_d) for nonacetylated aS falls within 0.1 nM to 0.7 μM depending on conditions (Dudzik et al., 2011), orders of magnitude weaker affinities have been determined for Cu(II) binding to N-terminally acetylated aS (K_d of 23 μM) (Teng et al., 2021). This means that at biological relevant concentrations of aS, that can reach 50–100 μM (Perni et al., 2017), Cu(II) interactions with aS may occur even with N-terminal acetylation. C-terminal residues (Glu123, Asp121, Asp119) are involved in weaker interactions between Cu(II) and the protein (mM affinity) that are not likely to be relevant at physiological conditions (Wittung-Stafshede, 2022; Rasia et al., 2005).

Despite clear links between copper dys-homeostasis and neurodegeneration involving amyloids, *there has been no studies of copper incorporation into, and copper binding to, aS amyloids*. We here fill this gap by characterizing Cu(II) interactions with amyloids formed by wild-type aS, N-terminally acetylated aS (perturbing free N-terminus) and the aS variant His50Ala (perturbing His50). The latter two variants were selected to specifically assess residues interacting strongly with Cu(II) in the monomeric protein. We reveal that wild-type and the two aS variants readily incorporate Cu(II) in the amyloids when Cu is supplied during aggregation, but a variant with both N-terminal acetylation and His50Ala mutation does not incorporate copper into the amyloids. There is a clear increase in binding capacity of the amyloids when Cu(II) is added before, as compared to after, amyloid formation. Chemical properties of Cu (redox activity and electrochemical potential) as well as amyloid morphology (fibril pitch, secondary structure, proteinase sensitivity)

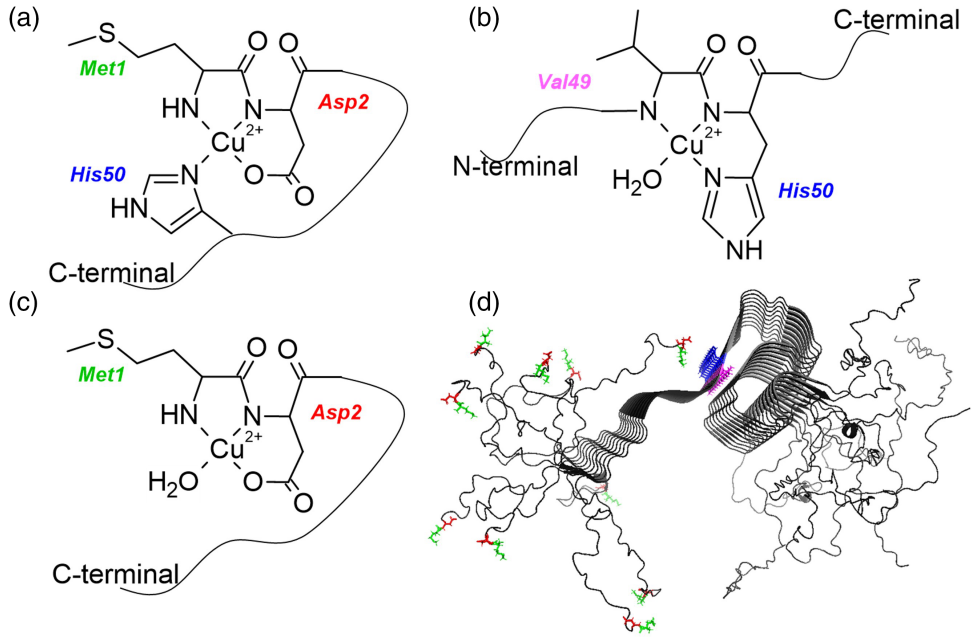

FIGURE 1 Possible Cu(II) coordination modes in monomeric aS. (a) Cu(II) coordination to the N-terminal site involving the N-terminal amino nitrogen of Met1, the deprotonated backbone amide, the carboxylate oxygen of Asp2, and the imidazole nitrogen of His50. (b) Cu(II) site around His50 as proposed for N-terminally acetylated aS with coordination to backbone nitrogens of Val49 and His50, the imidazole nitrogen of His50, and a water oxygen. (c) N-terminal site, as found in the membrane-bound form of the protein, involving the N-terminal amino nitrogen of Met1, the deprotonated backbone amide, the carboxylate oxygen of Asp2, and water molecule. (d) One (of many) reported high-resolution structures of aS amyloids (2N0A) with residues involved in high-affinity Cu binding to monomeric aS highlighted in sticks with colors as in a–c labels.

are altered when Cu is coordinated in amyloids of wild-type, N-terminally acetylated wild-type, and His50Ala aS proteins. Taken together, our data shows Cu(II) to be readily incorporated in aS amyloids even if the N-terminus is acetylated (as often found in vivo) or His50 is mutated (as found in the disease-causing variants His50Gln and His50Asp). Importantly, the formed amyloid–Cu complexes display alterations with respect to both protein and metal properties.

2 | RESULTS

We first re-evaluated the effect of Cu(II) on aS aggregation kinetics using the standard Thioflavin-T (ThT) assay. We here used wild-type aS (WT), N-terminally acetylated wild-type aS (Ac-WT), and the His50Ala variant of aS (H50A). All monomeric aS variants could bind one Cu(II) in a stoichiometric fashion (100 μM monomers) according to visible circular dichroism (CD) although Ac-WT showed a weaker signal change at 300 nm (Figure S1). The CD bands (ligand to metal charge transfer around 300 nm and (not shown for variants due to noise) d-d Cu(II) transitions at 600 nm) report on Cu(II) coordination to the protein. In accord, previous studies have reported affinity constants of Cu(II) to WT and H50A aS that are in the sub-nanomolar range (Dudzik et al., 2011) and Ac-WT was found to have a Cu(II) affinity in the low micromolar range (Teng et al., 2021). All aS variants readily formed amyloids, but with somewhat different kinetics. Cu(II) additions (0.5, 1, and 2 molar ratios to 50 μM aS monomers) accelerated aggregation of WT and, to a lesser some degree, H50A, whereas aggregation kinetics of Ac-WT was not affected, or somewhat slowed down (Figure S2). As a control, we investigated the copper-binding capacity of the aS variant containing both N-terminal acetylation and His50Ala mutation (Ac-H50A aS). For this aS variant, there was no evidence of Cu(II) binding to the monomer nor any effect of Cu on aggregation kinetics (Figures S1 and S2). This result demonstrates the absence of nonspecific (and/or C-terminal) Cu(II) binding to the aS variants at our experimental conditions.

As the effect on aggregation kinetics by Cu(II) does not necessarily reveal if the metal ion becomes bound or not in the resulting amyloids, we next set out to determine the amount of Cu associated with amyloid fibers upon completion of the reactions. For this, we

developed a method that takes advantage of Cu(I) detection by bicinchoninic acid (BCA). Resulting amyloids were spun down and protein as well as Cu were quantified. For the latter, BCA was added together with excess of ascorbic acid (to reduce Cu(II) to Cu(I)) and the formed BCA_2–Cu(I) complex was quantified by visible absorption (Figure S3). It is important to also quantify amount of resulting amyloids as aS aggregation never reaches full completion. We assessed two pathways: Cu added before aS aggregation and Cu added to the amyloids after their formation (Figure 2, top illustrations). In accord with a previous measurement (using 4-(2-pyridylazo) resorcinol) of Cu(II) in WT aS amyloids (Rasia et al., 2005), 70%–80% of added Cu is incorporated into WT aS amyloids (for ratios of 0.5 and 1 Cu: protein) when Cu is added before aggregation. Despite no accelerating effect on aggregation kinetics, also for Ac-WT amyloids are near-stoichiometric amounts of Cu incorporated into the amyloids when added at the start of the aggregation reaction (Figure 2a). In contrast to the monomer:Cu stoichiometry saturating at 1, when Cu is added during aggregation more than one Cu per monomer is incorporated into the resulting amyloids, with the most dramatic effect for Ac-WT amyloids (1.9 Cu per protein in the amyloids). This implies that Cu ions interacting with aS during aggregation access new binding sites not present in the monomer. In sharp contrast to WT and singly mutated aS variants, there was insignificant Cu incorporation into Ac-H50A amyloids (Figure 2a).

We then analyzed the amount of Cu bound to amyloids after Cu(II) addition to preformed amyloids. Here, amyloids (purified from any non-aggregated monomers) were incubated with various ratios of Cu(II) for 30 min followed by the same procedure of amyloid isolation and protein/Cu quantification as above for Cu(II) added before aggregation. Notably, we find similar Cu binding ability to WT amyloids for Cu addition after aggregation as when Cu was added prior to aggregation. In contrast, for Ac-WT and H50A variants, only sub-stoichiometric amounts of Cu(II) become bound to the amyloids when added after amyloid formation (Figure 2b). As expected,

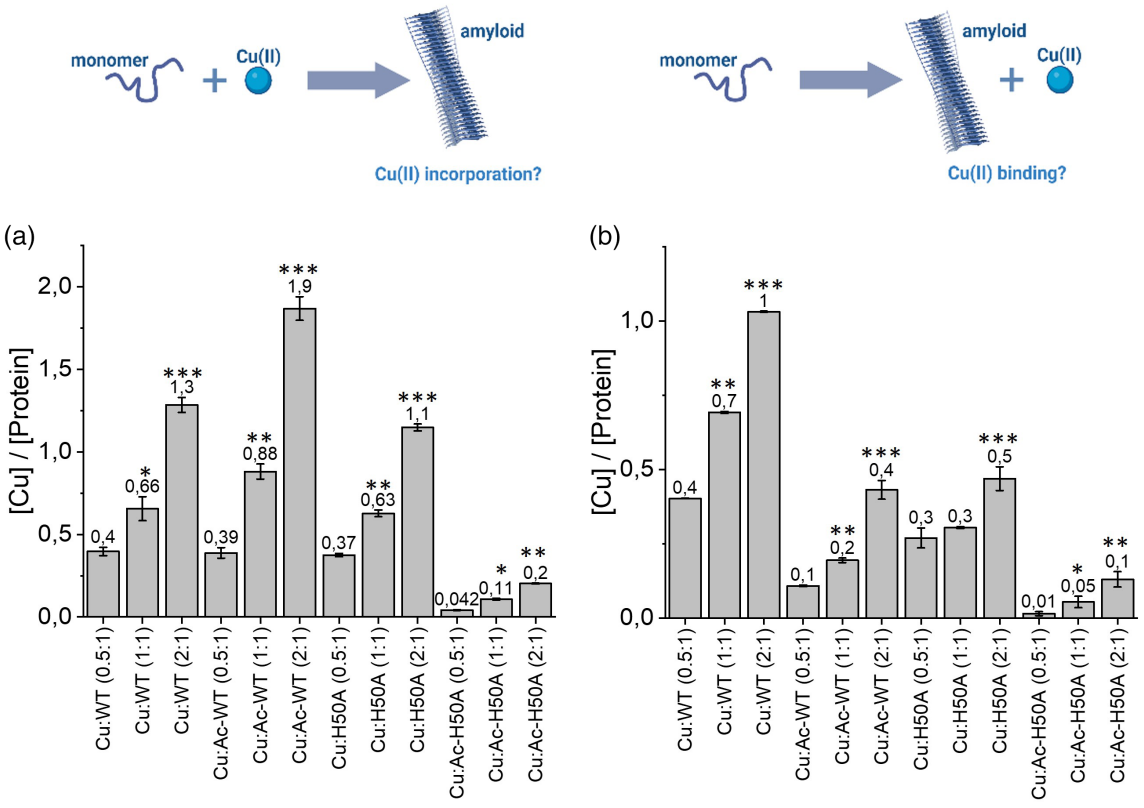

FIGURE 2 Quantification of Cu(II) binding to aS amyloids when added before or after amyloid formation. (a) Cu(II) incorporation into aS amyloids when added to monomers before aggregation. (b) Cu(II) binding to aS amyloids when added to aS after amyloid formation. Cu was added in indicated molar ratios to the monomeric/amyloidogenic protein at the start/end of the aggregation reaction (X-axis). The amounts of Cu in resulting amyloids (y-axis) were determined as described in Materials and Methods. At least three different experiments were performed for each condition/mixture. Initial protein concentration, 50 μM. Error bars, standard error of the mean. Significant differences derived upon comparing 0.5 eq. Cu added to the other two Cu(II) ratios for each aS variant. *$p < 0.05$; **$p < 0.01$; ***$p < 0.001$.

the Ac-H50A variant did not bind any Cu when Cu was added to preformed amyloids (Figure 2b). Interaction of Cu with preformed mutant amyloids may be a slow process (we only incubated for 30 min here), or the Cu binding sites that can be accessed during aggregation are not available when amyloids are pre-formed. Further studies on Ac-WT and H50A are required to determine the reason for the low Cu incorporation when the metal ions are added to preformed amyloid fibers. Taken together, amyloids of aS can interact with Cu(II) when mixed in micromolar concentrations. When Cu(II) is present during aS aggregation, there is efficient metal ion incorporation despite individual high-affinity Cu binding residues (in the monomers) being perturbed. For Ac-WT and H50A variants, Cu(II) levels in amyloids are higher when Cu(II) is added to monomers, before aggregation, as compared to Cu(II) addition (30 min incubation) to preformed amyloids. Thus, the binding sites available when Cu is present during aggregation of these aS variants become restricted from (quick) access in the final amyloids.

We then tested if amyloid morphologies (of WT, Ac-WT, and H50A amyloids) were affected by the incorporation of Cu(II) using atomic force microscopy (AFM) and far-UV CD. Indeed, the far-UV CD spectra, reporting on overall β-sheet content and β-strand arrangement, were found to differ in magnitude (for the same protein concentration) between amyloids formed without Cu(II) and those formed with Cu(II) present during the aggregation (Figure S4). Whereas the negative CD amplitude at 220 nm increased for WT amyloids when Cu was incorporated (suggesting more secondary structure but may also correspond to altered β-strand arrangement), the CD amplitude decreased (implying decrease in secondary structure but may also correspond to alterations in β-strand packing) when Cu had been incorporated into mutant aS amyloids. Nonetheless, the far-UV CD spectra indicated typical β-structure for all amyloids. Further support for structural changes due to Cu(II) came from AFM analysis of the amyloids. In Figure 3a, we show AFM images for the three aS amyloids, formed without and with the presence of 0.5 molar ratio of Cu(II). All amyloids showed fibril heights of around 6–8 nm, regardless of Cu(II), which is according to the literature for aS amyloids (Lorentzon et al., 2021). However, the twisting pattern (periodicity) along the fibers, denoted as a fiber pitch, varied between the three aS variants and if Cu had been added or not (Figures 3b and S5).

For WT amyloids, the dominant pitch value is around 70–80 nm, although some shorter pitches are also noted. For WT amyloids formed in the presence of Cu(II), the amyloid fiber pitch is increased to around 100–110 nm for the majority of fibers (Figure 3b). For H50A, the pitch of the amyloids without Cu(II) is centered around 100–110 nm. With Cu present during aggregation, the 100–110 nm value still dominates but also fibers with larger (120–130 nm) and shorter (70–80 nm) pitches are detected (Figure 3b). Ac-WT amyloids display two pitch values without Cu: 75–85 nm and 95–105 nm. With Cu present during aggregation, the high pitch value disappears at the expense of a new pitch value of 45–55 nm for the resulting amyloids (Figure 3b). Importantly, in these experiments, we added 0.5 equivalent of Cu and thus we do not expect all amyloids to be fully loaded with Cu. It is thus reasonable to find a combination of pitch values representing both amyloids with and without Cu(II) bound.

The pitch value depends on the specific aS amyloid fold and how two protofilaments twist around each other. Many external (buffer, salt, pH, additions) and internal (mutations, post-translational modifications) may affect the amyloid core structure and thereby the observed pitch. A set of pitch values reported for aS amyloids are summarized in Table S1 in our previous paper (Lorentzon et al., 2021). Typically, WT aS amyloids show pitch values around 100 nm; Ac-WT amyloids have been reported to have both larger and shorter pitches than amyloids of the protein without N-terminal acetylation (Lorentzon et al., 2021). In similarity to what we found for Cu(II) incorporation here, addition of As(III) or Cd(II) to Ac-WT aS during aggregation resulted in altered pitch values for the resulting metal-containing aS amyloids (Lorentzon et al., 2021).

Another way to assess structural changes in the amyloids is to probe sensitivity of the amyloids to protease degradation. Proteinase K digestion has been used to study structural variations in amyloid fibers and degradation pattern variations (time-dependence, fragment sizes) have been linked to different amyloid core structures and/or polymorphs (Landureau et al., 2021; Guo et al., 2013). When we compared Proteinase K degradation patterns of aS amyloids formed with and without Cu(II) (Figure S6), we find the digestion 'fingerprints' to differ. There are distinctions in both the time-dependence of fragments emerging and what fragments dominate during digestion. Interestingly, for WT and H50A amyloids with Cu, there appears to be a quick initial digestion that results in fragments that are stable with time. In contrast, amyloids without Cu (and Cu-loaded Ac-WT amyloids) are degraded more 'gradually' (many fragments of different sizes) and to a larger extent. Perhaps Cu incorporation makes some peptide loops more susceptible to cleavage but the core structure becomes more protected. Taken together, aS amyloids (WT, Ac-WT, and H50A) formed in the presence of Cu(II) adopt altered amyloid structure/morphology according to three experimental methods.

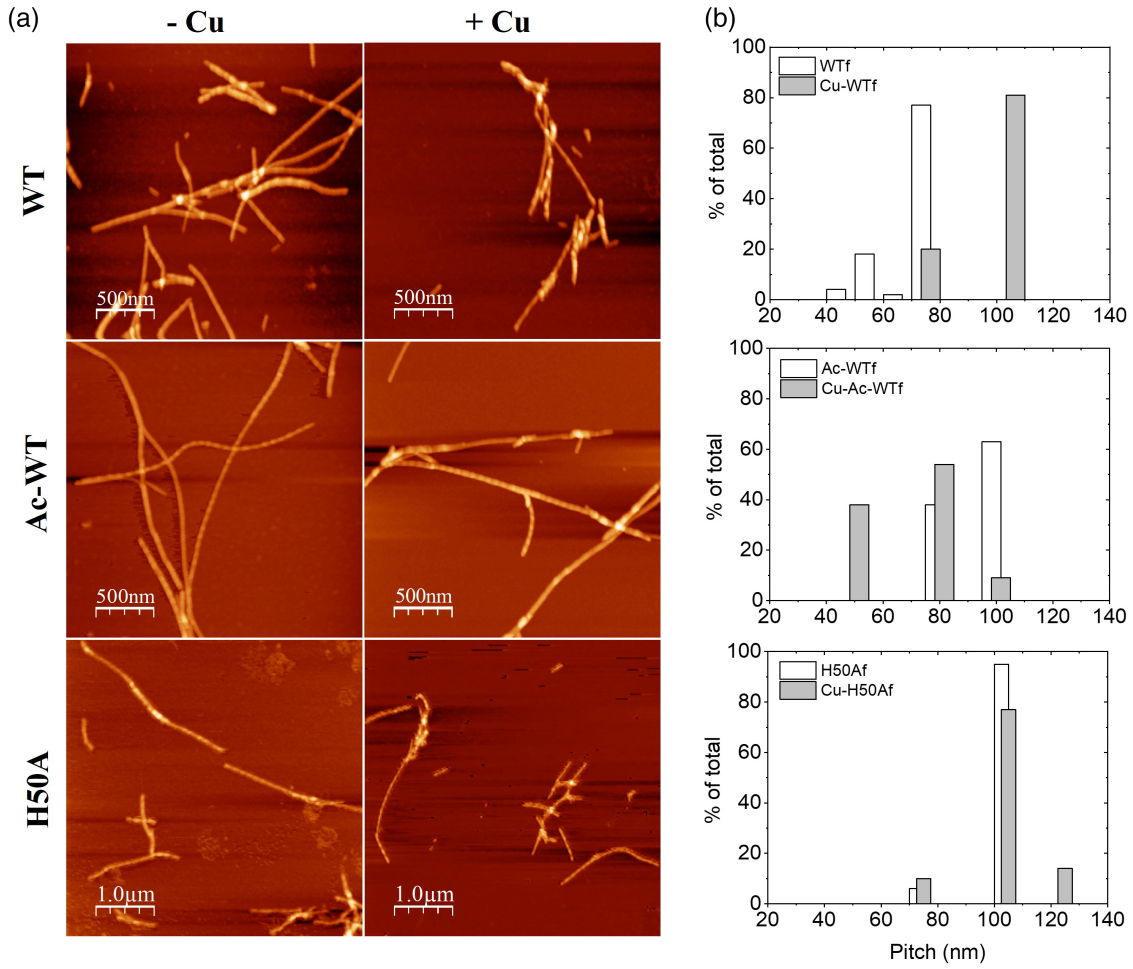

FIGURE 3 AFM analysis of aS amyloids. (a) AFM images of WT, Ac-WT and H50A aS amyloids with (+Cu) and without (−Cu) 0.5 molar ratio of Cu(II) added at the start of the aggregation reactions. Thus, it is expected that each +Cu amyloid sample here is a mixture of amyloids with Cu and amyloids without Cu (according to data in Figure 1). (b) Distribution of fiber pitch values with and without Cu. The pitch was measured as the distance between two maxima in the height curves (see Figure S5). Total number of amyloids evaluated per sample was 30–60 fibers. Histogram bin size is 10 nm.

Next, we turned to the chemical properties of Cu when incorporated into aS amyloids (WT, Ac-WT, and H50A). With cyclic voltammetry (CV), the Cu redox potential can be determined which provides information on redox reversibility, reactivity, and what redox state, Cu(II) or Cu(I), is most favored in the coordination environment. In Figure 4, we show voltammograms for Cu-bound monomers and amyloids of the aS variants. CV experiments were performed on samples with matching Cu concentrations (200 µM). The samples with Cu bound to amyloids showed reduced overall current and increased separation between oxidation and reduction peaks as compared to Cu bound to monomers (Table S1), indicative of an increased barrier for electron transfer.

Despite the sluggish data, the reduction–oxidation reactions were reversible, and the current depended (in most cases) linearly on the square root of the scan rate (Figure 4) as expected for a freely diffusing species (Elgrishi et al., 2018). This implies that Cu is stably bound to the amyloids in both redox states. In Table S1, we list the estimated $E_{1/2}$ values versus Ag/AgCl as a reference for all Cu–aS complexes. The redox potential determined here for Cu in the WT aS monomer (0.016 V) is similar to a reported $E_{1/2}$ value (0.018 V) for this complex (Wang et al., 2010). For Cu in the amyloids, the $E_{1/2}$ values shift to more negative values as compared to Cu in the monomers (Table S1). More negative redox potential implies that the oxidized state is favored over the reduced state, and the metal ion is thus harder to reduce when bound in amyloids as compared to when bound to monomers. All redox potentials measured for Cu–aS complexes, although they vary between samples, fall in a range that would allow for Cu reduction by reducing agents such as glutathione and ascorbic acid (Wang et al., 2010). Importantly, the latter compounds are present in the brain in high

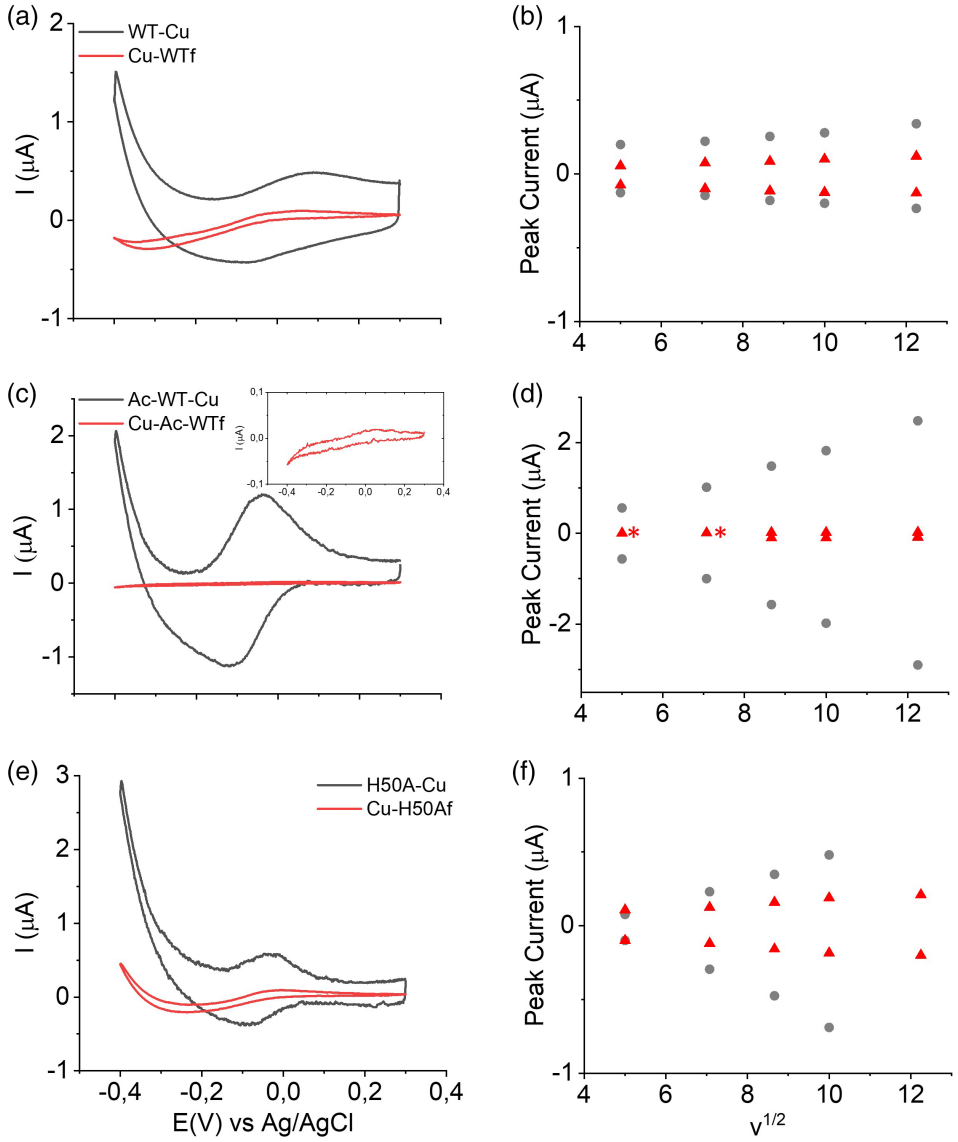

FIGURE 4 Electrochemical properties of Cu in aS amyloids. CV of Cu bound to monomeric aS (Cu-WT), and Cu in amyloids formed with Cu(II) present at the start of aggregation (f indicates fiber) for WT (a), Ac-WT (c) and H50A (e) at a scan rate of 50 mV/s. Inset in C shows an enlarged CV of Cu incpoporated in Ac-WT amyloids (to make peak features visible). Relationships between peak current and square root of scan rate (from 25 mV/s to 150 mV/s) for WT (b), Ac-WT (d) and H50A (f). For Ac-WT the two * indicate that only one of the peak currents was possible to measure. Estimated midpoint potentials ($E_{1/2}$), peak-to-peak separation (ΔE), and ratio of peak currents are reported in Table S1.

concentrations and are biological reducing agents (Forman et al., 2009; Smirnoff, 2000).

Free Cu ions are highly reactive and can generate ROS (such as hydroxyl radicals, $^{\bullet}$OH) via Fenton chemistry in the presence of oxygen and a reducing agent (that (re)generates Cu(I)) (Figure 5a). Cu(II) bound to monomeric aS has been reported to have some redox activity (Pedersen et al., 2016), although less than free metal ions. To compare Cu reactivity when bound to amyloids versus bound to aS monomers, we employed a fluorescent reporter probe, 3-coumarin carboxylic acid (3-CCA). 3-CCA scavenges hydroxyl radicals to form the fluorescent product 7-OH-3-CCA ($\lambda_{Ex} = 395$ nm, $\lambda_{Em} = 450$ nm). Because of the non-fluorescent nature of 3-CCA and its high hydroxylation rate constant, the detection of 7-OH-CCA allows for real-time measurements of $^{\bullet}$OH generation (Manevich et al., 1997). In Figure 5b, we show the kinetics of $^{\bullet}$OH formation in the presence of monomeric as well as amyloid forms of WT aS formed in the presence of Cu(II) and the reducing agent ascorbic acid (that upon generation of Cu(I) initiates the reaction cycle) (variant aS kinetics are shown in Figure S7). The amount of $^{\bullet}$OH generated after 100 min of reaction for monomeric as well as amyloid forms of the three aS variants with Cu(II) and ascorbic acid is compared in Figure 5c.

Cu alone shows the highest tendency to generate $^{\bullet}$OH radicals. Cu bound to aS monomers display less reactivity than free Cu but higher reactivity than Cu bound to amyloid fibers (Figure 5c). Thus, Cu incorporation in amyloids shields the metal ion from ROS generation as compared to when bound to aS monomers or free in solution. The 'inertness' of Cu in amyloids is reasonable as a high reorganization energy for Cu(II)/Cu(I) transitions (involving two markedly different coordination spheres) is expected within a rigid scaffold such as an amyloid fiber.

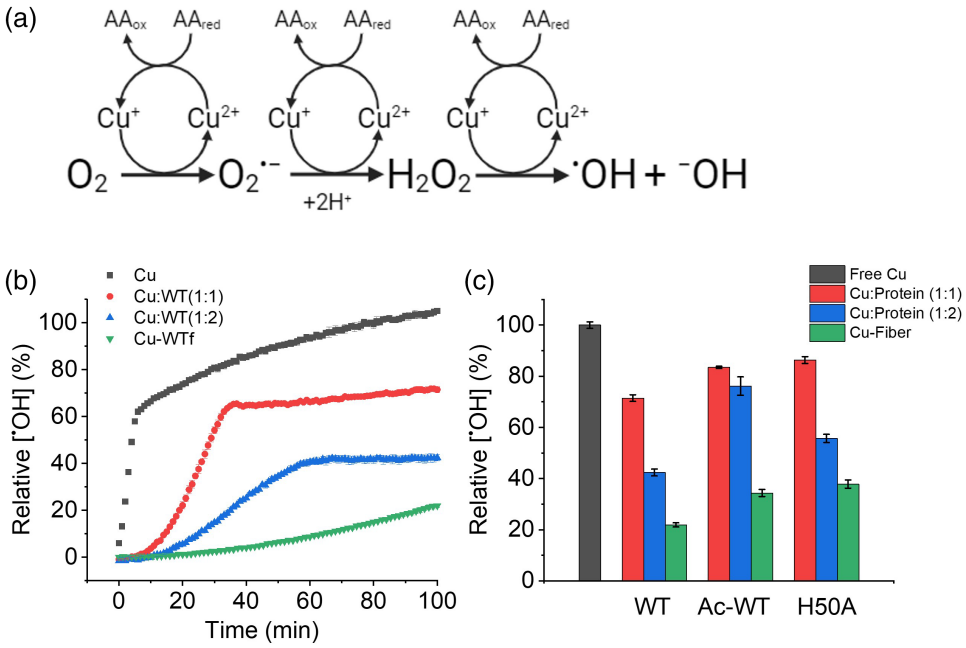

FIGURE 5 ROS generation by Cu in aS amyloids. (a) Scheme representing proposed mechanism for Cu-induced ROS production in the presence of oxygen and reducing agent. (b) Hydroxyl radical (•OH) production (detected by fluorescence upon oxidation of 3-CCA) by free Cu and Cu bound to WT aS monomers (1:1 and 1:2 Cu to monomer molar ratios) as well as for Cu in WT aS amyloids (Cu added before amyloid formation, f indicates fibers). Background signals from CCA and ascorbic acid was subtracted. (c) •OH production (at 100 min) by Cu bound to monomeric and amyloid forms of WT (kinetic data in "b"), H50A aS and Ac-WT aS as indicated (kinetic data for H50A and Ac-WT aS shown in Figure S7). The concentration of Cu in all samples was 10 μM. The experiments were performed in triplicates and repeated at least two times.

3 | DISCUSSION

Parkinson's disease and many other neurodegenerative disorders are coupled to altered cellular and systemic copper levels as well as to cellular oxidative stress. Since many of the amyloidogenic proteins, forming the hallmark amyloids found in patients with these diseases, can bind copper ions, it is of importance to better understand consequences of copper binding to amyloids. In this work, we have discovered that Cu(II) becomes incorporated into α-synuclein amyloids. If Cu is added before protein aggregation, the metal ion is readily incorporated in resulting amyloids also if the N-terminus of aS is acetylated or His50 is perturbed. This is of biological significance as aS is often N-terminally acetylated in vivo and His50 is mutated in many disease-causing variants of aS. If Cu is added after amyloids are formed, only a small fraction of Cu(II) readily binds copper-site aS variants Ac-WT and H50A.

When Cu gets incorporated into amyloids, WT, Ac-WT, and H50A, the amyloid morphology/structure is altered as deduced from amyloid pitch analysis by AFM, far-UV CD, and proteinase K sensitivity. It has also been reported that the FTIR spectrum (amide-I region) is altered when aS amyloids are formed in presence of Cu(II) (1:5 aS:Cu ratio was used without removing remaining monomers or Cu ions from resulting amyloids) (Atarod et al., 2022). Thus, it appears that early Cu incorporation results in an altered (imprinted) aS amyloid structure. At the same time, the reduction potential (CV) and redox reactivity (ROS generation) of Cu is altered when incorporated into amyloid fibers as compared to when bound to monomer aS. The reduction potential is shifted to more negative values and the Cu is less susceptible towards ROS generation when bound in amyloids as compared to when bound to monomers. Since these effects on Cu chemical properties in amyloids of WT, Ac-WT, and H50A proteins are similar, it implies that the Cu coordination (but not necessarily the specific residues) within the amyloid fold is comparable in all three amyloids, and thus does not depend explicitly on the N-terminus or His50. Still, these residues are likely critical for Cu binding as the variant Ac-H50A did not incorporate any Cu into its amyloids.

Whereas His50 is positioned in the amyloid ordered core (with the His side chain exposed on the core outside), the N-terminus is part of the 'fuzzy coat' that, together with the C-terminus, remain disordered in the amyloid structure. The data presented show that Cu binding to the N-terminus (H50A variant) or to His50

(Ac-WT) of aS monomers allows the metal to get incorporated into the amyloids during aggregation. In the resulting amyloids, Cu may remain coordinated to one of the (monomer) sites along with formation of additional interactions with residues spatially nearby in the amyloid structure. Cu coordination to His50 may induce ordering of N- or C-terminal floppy stretches to form a fully coordinated Cu site. Cu bound to the N-terminus may result in its folding onto the amyloid core via additional Cu interactions with core residues. In agreement with these scenarios, an elegant study combining cryo-EM and ssNMR recently reported that when a scaffold protein bound to floppy C-terminal residues in aS amyloids, the N-terminal floppy part folded onto the amyloid core resulting in an amyloid with more β-strands (Zhang et al., 2023). High-resolution structural studies of aS amyloids formed in the presence of Cu are required to address these speculations. In addition, electronic paramagnetic resonance (epr) analysis of the Cu electronic configuration in the various aS variant amyloids is another way to identify possible coordination ligands (work in progress).

Earlier reports on both aS and amyloid-β (the peptide assembling to amyloids in Alzheimer's disease) (Wang et al., 2010; Pedersen et al., 2016) are in agreement with our observation of attenuated ROS generation when Cu is bound to amyloids as compared to free Cu and, to a lesser extent, when Cu is bound to the monomers. There has been no quantitative/structural studies previously on Cu(II) binding to aS amyloids, but there are a few such studies on amyloids of amyloid-β and IAPP (the amyloidogenic peptide in type-2 diabetes). It was reported that Cu(II) coordination, as defined by epr, in monomeric and amyloid forms of amyloid-β were identical (Karr et al., 2004) and a model for Cu(II) binding in amyloid-β amyloids was proposed to involve alternating Cu(II) sites on both sides of the amyloid (Gunderson et al., 2012). Importantly, this coordination structure was not conductive to redox-linked coordination changes and could thus explain why Cu redox cycling was suppressed. Unlike amyloid-β and aS, where Cu(II) can speed up amyloid formation, studies have shown that Cu(II) binding to IAPP monomers delayed amyloid formation (Rivillas-Acevedo et al., 2015). Still, Cu(II) became bound to the resulting IAPP amyloids that formed slower, and also Cu added to preformed amyloids of IAPP could bind. Using epr, it was shown that Cu(II) binding sites in amyloids and monomers of IAPP involved different Cu coordination (Rivillas-Acevedo et al., 2015).

In Parkinson's disease, cellular Cu is lowered but Cu levels in blood and CSF is increased (Bush, 2000; Bisaglia & Bubacco, 2020). At the same time, occupational exposure to high levels of Cu is toxic and may result in Parkinson's disease (Bisaglia & Bubacco, 2020). One possibility is that bioavailable cellular Cu gets incorporated into aS amyloids and in this way, Cu is removed from the intracellular pool. Since SOD1, the major antioxidant in cells depends on Cu (Banci et al., 2013), its activity will go down with lowered cellular Cu and oxidative stress is initiated. It may also be possible that oxidative stress comes first and this causes free Cu(II) ions in the cell that induce aS amyloid formation. In this scenario, Cu binding to the amyloids would reduce negative consequences, and reactivity, of free Cu ions. Nonetheless, Cu would still be removed from the bioavailable pool by amyloid incorporation. Further studies are required that also involve copper transport proteins as at normal conditions, there is never any free Cu in the cell; all Cu is transported by dedicated Cu transporters (Wittung-Stafshede, 2022; Horvath et al., 2018). We showed recently that the cytoplasmic Cu chaperone Atox1 can form a ternary complex with aS, bridged by Cu(I) that inhibits amyloid formation (Horvath et al., 2019).

Today, many high-resolution structures of amyloids have been described and it clear that there are many amyloid folds possible for the same protein sequence (Sawaya et al., 2021). Metal ions, such as Cu (shown here, but also As(III) and Cd(II) (Lorentzon et al., 2021)), may be responsible for some of the structural diversity of aS amyloids, along with effects of other environmental factors. The connection between amyloid polymorph and pathological consequences may be related to differences in cell–cell spreading and toxicity among amyloid polymorphs. It has been reported that aS amyloids (formed in the presence of 5-fold excess Cu(II)) are more toxic to cells than amyloids without Cu(II) while the same amount of free Cu has no toxic effect (Atarod et al., 2022). Recent work has shown that amyloids of aS and amyloid-β harbor catalytic activity (Horvath & Wittung-Stafshede, 2023) and such activities may be tuned by metal ion interactions. Further structural and cellular studies are required to pinpoint the biological relevance of the putative connection between copper and amyloids in Parkinson's disease and in other neurodegenerative disorders.

4 | MATERIALS AND METHODS

4.1 | Protein expression and purification

The human WT aS and H50A aS variants were transformed into BL21 (DE3) (Novagen) cells. Transformants were first grown to an OD_{600} of 0.6 in LB containing 100 μg/mL carbenicillin at 37°C, then induced with 1 mM isopropyl b-D-1-thiogalactopyranoside (IPTG) and grown overnight at 20°C. Cells were lysed by sonication

in pulse mode in 20 mM Tris–HCl buffer pH 8.0 in the presence of protease inhibitor cocktail (Roche) in an ice bath. After sonication, the lysate was treated with a universal nuclease (Pierce) for 15 min at room temperature. The lysate was then heated at 90°C for 10 min followed by centrifugation for 30 min at 15,000 g. The centrifuged lysate after filtration (Nalgene rapid-flow filter, 0.2 µm PES membrane; Thermo Fisher Scientific) was loaded on a pre-equilibrated 5 mL HiTrap Q FF anion exchange column (Cytvia) and eluted by a linear gradient of 1 M NaCl in 20 mM Tris–HCl, pH 8.0. Fractions contained the protein were combined and concentrated with Ultra-15 Ultracel 10 K centrifugal filtration devices (Millipore). The concentrate was then loaded on to HiLoad 16/600 Superdex 75 pg column (Cytvia) and retrieved in 20 mM Tris-sulfate buffer, pH 7.4. Purity was confirmed by a single-band on SDS-PAGE gel and a single elution peak in SEC. Protein samples were flash frozen and stored at −80°C until use. To determine protein concentration, the extinction coefficient of 5960 M^{-1} cm^{-1} at 280 nm was used. N-terminally acetylated WT aS and N-terminally acetylated H50A aS was purified following the previously published protocol (Lorentzon et al., 2021). The two proteins were overexpressed by co-transforming their respective plasmids with pNatB (a kind gift of D. P. Mulvihill (Johnson et al., 2013)) in BL21 (DE3) (Novagen) cells, co-expressing the yeast N-acetyltransferase NatB gene. After expression, the proteins were purified using the same protocol as for non-acetylated aS described above and resulted in fully N-terminally acetylated aS protein (WT and H50A) as confirmed by mass spectrometry.

4.2 | Stock preparations

A stock solution of Cu(II) (100 mM) was prepared in Milli-Q water from $CuCl_2{\cdot}2H_2O$ (Merck) and then further diluted for the different experiments. We verified stock concentration from the Cu(II) d-d absorption at 780 nm ($\varepsilon = 12\ M^{-1}\ cm^{-1}$). Ascorbic acid and bicinchoninic acid (BCA) solutions (Merck) were prepared by dissolving a known amount of respective powder in MQ water. 3-coumarin carboxylic acid (CCA) stock solution was prepared by dissolving a known amount of powder in a small volume of 20 mM phosphate buffer, pH 9, followed by dilution with 20 mM phosphate buffer, pH 7.4 to make a 10 mM stock solution.

4.3 | ThT assay

The amyloid formation assays were conducted using 96-well half-area transparent bottom plates (CLS3881; Corning, Corning, NY, USA), with 2 mm glass bead in each well in a plate reader-incubator instrument (Fluostar Optima; BMG Labtech, Ortenberg, Germany). To prevent contamination and evaporation, the plates were sealed with transparent tape. Measurements were performed in TBS (0.05 M Tris–HCl buffer, pH 7.4 with 0.15 M NaCl, Sigma-Aldrich, St. Louis, MO, USA) in the presence of 20 µM Thioflavin T (ThT; T3516; Sigma-Aldrich, St. Louis, MO, USA) at 37°C using 5 min 200 rpm agitation at the beginning of each 20 min measurement cycle. Fluorescence was measured from the bottom of the plate. aS was gel-filtered on a Superdex S75 10/300 GL (Cytvia) before each experiment to ensure that the starting point was pure monomers. Experiments were performed with 4–5 replicates and repeated three independent times. Each time, samples with ThT present and absent were run in parallel. The samples without ThT were used for further experiments (see below).

4.4 | Estimation of Cu in amyloids using BCA

After aggregation kinetics followed in the plate reader, samples without ThT were placed in Eppendorf tubes and centrifuged for 30 min at 13 k rpm to obtain the amyloid fibers in pellet form. Then supernatant containing the monomeric/non-fibrillar protein and possible free Cu(II) was collected. The protein concentration in the supernatant was determined using absorbance at 280 nm. To estimate the Cu(II) concentration in the supernatant, we added four equivalents of BCA and 10 equivalents of ascorbic acid (to reduce Cu(II) to Cu(I)) and vortexed for 2 min and incubated for 30 min at room temperature. Absorption at 562 nm, which corresponds to $(BCA)_2$-Cu (I) (extinction coefficient of 7700 M^{-1} cm^{-1}), was measured to determine the Cu content in the supernatant. As the total protein and Cu concentrations at the start of the experiment are known, the amount of amyloids and their Cu content can be determined.

4.5 | Atomic fluorescence microscopy (AFM)

Samples from the ThT aggregation assays at 90 h were diluted 10 times in MilliQ water and deposited onto freshly cleaved mica. After 15 min, the mica samples were rinsed 3–4 times with MilliQ water then dried completely under a gentle stream of nitrogen gas. The images were captured using an NTEGRA Prima setup (NT-MDT, Moscow, Russia) at a resonance frequency around 180 kHz, using a gold-coated single crystal silicon

cantilever (NSG01, spring constant of ~5.1 N/m; NT-MDT, Moscow, Russia). Images of 512 pixels were captured at a scan rate ranging from 0.3–0.5 Hz. Images were analyzed using WSxM 5.0 software.

4.6 | Circular dichroism (CD)

CD was measured in the far-UV (190–250 nm) and visible region (250–700 nm) on Chirascan-CS spectrophotometers using a 0.1 and 1 cm quartz cuvette, respectively, at 20°C. In the visible region, 100 μM aS monomers in TBS buffer, pH 7.4, were titrated with Cu(II) from 1:0.25 to 1:2 protein:Cu(II) ratios, with approximately 10 min incubation between each addition. Amyloid fibers of aS variants were produced with and without two equivalents of Cu (purification and quantification described above); then analyzed (protein concentration of 10 μM; 10 mM phosphate buffer, pH 7.4) in the far-UV region. Each experiment was repeated three times.

4.7 | Proteinase K sensitivity

Amyloid fibers of aS variants were produced with and without two equivalents of Cu (see above). Proteinase K enzyme (4 μg/mL) (Thermo Fischer Scientific) was added to 100 μM aS amyloid samples (total volume 100 μL) at 37°C. Aliquots (20 μL) were removed at different time points (0.5, 1, 5, 15, and 30 min) and transferred into centrifuge tubes containing proteinase K inhibitor, PMSF (phenylmethyl sunfonyl fluoride, Merck). The samples were dried by speed vacuum and then amyloids were dissolved into monomers using HFIP (1,1,1,3,3,3-Hexafluoroisopropanol, Merck). After evaporation of HFIP, samples were dissolved in sample loading buffer and heated for 5 min at 90°C before SDS-PAGE (12%) analysis. Control experiments without the addition of Proteinase K, but following the same procedure, were also analyzed by SDS-PAGE.

4.8 | Preparation of amyloids with Cu added before aggregation (for CV and CCA)

100 or 200 μM of protein was incubated with two equivalents of Cu(II) for 4–6 days at 37°C with constant shaking (500 rpm) to complete the aggregation process. 0.02% NaN_3 was added in the samples to prevent the bacterial growth. Next the amyloids were collected via centrifugation (30 min, 13,200 rpm) and the resulting pellet washed 2–3 times with buffer before being resuspended into an appropriate volume of buffer. Concentrations of protein and Cu in the amyloids were calculated using protein absorption and BCA experiments as described above (using the first supernatant, before washing). The amyloid samples were then dissolved with buffer to reach a final concentration of Cu of 0.2 mM/10 μM (CV/CCA).

4.9 | Cyclic voltammetry (CV)

Cyclic voltammetry was carried out using Electrochemical Analyzer CH 600B model. Screen Printed Carbon Electrode (SPCE) model 150 purchased from Metrohm DropSens was used which consists of carbon (4 mm) as working, platinum as counter electrode and Ag/AgCl as reference electrode. SPCEs were subjected to pretreatment before use following previously reported protocol (Domínguez-Aragón et al., 2023). Briefly, this involved chronoamperometry using a fixed potential at −1 V during 150 s followed by a +1 V potential during 150 s in TBS, pH 7.4, as the electrolyte. Then, CV was performed from 0 to 0.8 V at a scan rate of 100 mV/s for 20 cycles. All sample solutions were thoroughly purged with nitrogen gas prior to recording data. The experiments were carried out at room temperature with different scan rates 25, 50, 75, 100, and 150 mV/s. In all CV experiments, the Cu concentration was adjusted to 0.2 mM. For amyloid samples, this means that the actual protein concentration may be somewhat higher as Cu did not get incorporated to 100%, see below for how samples were prepared.

4.10 | Coumarin carboxylic acid (CCA) assay

CCA was used to detect hydroxyl radicals (•OH). •OH generated reacts with CCA to form 7-hydrioxy-coumarin-3-carboxylic acid (7-OH-CCA), which upon excitation at 390 nm emits at 450 nm. To 20 mM phosphate buffer with 0.15 M NaCl, pH 7.4, solutions containing 0.2 mM CCA, 10 μM Cu(II) alone or combined with aS monomers (ratios Cu(II):aS of 1:1 and 1:2) or Cu-loaded amyloids, ascorbic acid was added to trigger the reaction (0.2 mM). Amyloid fibers with Cu added before and after aggregation were prepared as explained above and all samples had a Cu concentration of 10 μM. Kinetics of •OH generation was measured via fluorescence at 450 nm in black 96-well optical bottom plates (Corning) Fluostar Optima plate reader (BMG Labtech, Ortenberg, Germany). Experiments were performed in triplicates at least two times on different days. No significant differences were observed, and Figure 3 and Figure S7 therefore show representative measurements.

AUTHOR CONTRIBUTIONS

Gulshan Walke: Investigation; conceptualization; methodology; writing – review and editing; visualization. **Ranjeet Kumar:** Investigation; resources. **Pernilla Wittung-Stafshede:** Conceptualization; funding acquisition; writing – original draft; writing – review and editing; resources; supervision; investigation; methodology.

ACKNOWLEDGMENTS

We acknowledge funding from the Knut and Alice Wallenberg Foundation and the Swedish Research Council (PWS). We thank high-school students Sofie Anagrius Teodorsson, Klara Stenberg, and Elin Norström for performing preliminary experiments as part of a high-school research project.

CONFLICT OF INTEREST STATEMENT

The authors declare no conflict of interest.

ORCID

Pernilla Wittung-Stafshede https://orcid.org/0000-0003-1058-1964

REFERENCES

Aaseth J, Dusek P, Roos PM. Prevention of progression in Parkinson's disease. Biometals. 2018;31(5):737–47.

Atarod D, Mamashli F, Ghasemi A, Moosavi-Movahedi F, Pirhaghi M, Nedaei H, et al. Bivalent metal ions induce formation of alpha-synuclein fibril polymorphs with different cytotoxicities. Sci Rep. 2022;12(1):11898.

Banci L, Cantini F, Kozyreva T, Rubino JT. Mechanistic aspects of hSOD1 maturation from the solution structure of Cu(I) -loaded hCCS domain 1 and analysis of disulfide-free hSOD1 mutants. Chembiochem Eur J Chem Biol. 2013;14(14):1839–44.

Binolfi A, Rasia RM, Bertoncini CW, Ceolin M, Zweckstetter M, Griesinger C, et al. Interaction of alpha-synuclein with divalent metal ions reveals key differences: a link between structure, binding specificity and fibrillation enhancement. J Am Chem Soc. 2006;128(30):9893–901.

Binolfi A, Rodriguez EE, Valensin D, D'Amelio N, Ippoliti E, Obal G, et al. Bioinorganic chemistry of Parkinson's disease: structural determinants for the copper-mediated amyloid formation of alpha-synuclein. Inorg Chem. 2010;49(22):10668–79.

Binolfi A, Valiente-Gabioud AA, Duran R, Zweckstetter M, Griesinger C, Fernandez CO. Exploring the structural details of Cu(I) binding to alpha-synuclein by NMR spectroscopy. J Am Chem Soc. 2011;133(2):194–6.

Bisaglia M, Bubacco L. Copper ions and Parkinson's disease: why is homeostasis so relevant? Biomolecules. 2020;10(2):195.

Bjorklund G, Hofer T, Nurchi VM, Aaseth J. Iron and other metals in the pathogenesis of Parkinson's disease: toxic effects and possible detoxification. J Inorg Biochem. 2019;199:110717.

Bush AI. Metals and neuroscience. Curr Opin Chem Biol. 2000;4(2):184–91.

Bush AI. The metallobiology of Alzheimer's disease. Trends Neurosci. 2003;26(4):207–14.

Camponeschi F, Valensin D, Tessari I, Bubacco L, Dell'Acqua S, Casella L, et al. Copper(I)-alpha-synuclein interaction: structural description of two independent and competing metal binding sites. Inorg Chem. 2013;52(3):1358–67.

Carboni E, Lingor P. Insights on the interaction of alpha-synuclein and metals in the pathophysiology of Parkinson's disease. Metallomics. 2015;7(3):395–404.

Cheignon C, Tomas M, Bonnefont-Rousselot D, Faller P, Hureau C, Collin F. Oxidative stress and the amyloid beta peptide in Alzheimer's disease. Redox Biol. 2018;14:450–64.

D'Ambrosi N, Rossi L. Copper at synapse: release, binding and modulation of neurotransmission. Neurochem Int. 2015;90:36–45.

de Ricco R, Valensin D, Dell'Acqua S, Casella L, Gaggelli E, Valensin G, et al. Differences in the binding of copper(I) to alpha- and beta-synuclein. Inorg Chem. 2015;54(1):265–72.

Dev KK, Hofele K, Barbieri S, Buchman VL, van der Putten H. Part II: α-synuclein and its molecular pathophysiological role in neurodegenerative disease. Neuropharmacology. 2003;45(1):14–44.

Domínguez-Aragón A, Conejo-Dávila AS, Zaragoza-Contreras EA, Dominguez RB. Pretreated screen-printed carbon electrode and Cu nanoparticles for creatinine detection in artificial saliva. Chemosensors. 2023;11(2):102.

Dudzik CG, Walter ED, Millhauser GL. Coordination features and affinity of the Cu(2)+ site in the alpha-synuclein protein of Parkinson's disease. Biochemistry. 2011;50(11):1771–7.

Elgrishi N, Rountree KJ, McCarthy BD, Rountree ES, Eisenhart TT, Dempsey JL. A practical beginner's guide to cyclic voltammetry. J Chem Educ. 2018;95(2):197–206.

Fink AL. The aggregation and fibrillation of alpha-synuclein. Acc Chem Res. 2006;39(9):628–34.

Forman HJ, Zhang H, Rinna A. Glutathione: overview of its protective roles, measurement, and biosynthesis. Mol Aspects Med. 2009;30(1–2):1–12.

Fusco G, Pape T, Stephens AD, Mahou P, Costa AR, Kaminski CF, et al. Structural basis of synaptic vesicle assembly promoted by α-synuclein. Nat Commun. 2016;7:12563.

Gaier ED, Eipper BA, Mains RE. Copper signaling in the mammalian nervous system: synaptic effects. J Neurosci Res. 2013;91(1):2–19.

Galvin JE, Lee VM, Schmidt ML, Tu PH, Iwatsubo T, Trojanowski JQ. Pathobiology of the Lewy body. Adv Neurol. 1999;80:313–24.

Goldberg MS, Lansbury PT. Is there a cause-and-effect relationship between alpha-synuclein fibrillization and Parkinson's disease? Nat Cell Biol. 2000;2(7):E115–9.

Gray HB. Biological inorganic chemistry at the beginning of the 21st century. Proc Natl Acad Sci U S A. 2003;100(7):3563–8.

Gunderson WA, Hernandez-Guzman J, Karr JW, Sun L, Szalai VA, Warncke K. Local structure and global patterning of Cu2+ binding in fibrillar amyloid-beta [Abeta(1-40)] protein. J Am Chem Soc. 2012;134(44):18330–7.

Guo JL, Covell DJ, Daniels JP, Iba M, Stieber A, Zhang B, et al. Distinct alpha-synuclein strains differentially promote tau inclusions in neurons. Cell. 2013;154(1):103–17.

Horvath I, Blockhuys S, Sulskis D, Holgersson S, Kumar R, Burmann BM, et al. Interaction between copper chaperone

Atox1 and Parkinson's disease protein alpha-Synuclein includes metal-binding sites and occurs in living cells. ACS Chem Neurosci. 2019;10:4659–68.

Horvath I, Werner T, Kumar R, Wittung-Stafshede P. Copper chaperone blocks amyloid formation via ternary complex. Q Rev Biophys. 2018;51:e6.

Horvath I, Wittung-Stafshede P. Amyloid fibers of alpha-synuclein catalyze chemical reactions. ACS Chem Neurosci. 2023;14:603–8.

Johnson M, Geeves MA, Mulvihill DP. Production of amino-terminally acetylated recombinant proteins in *E. coli*. Methods Mol Biol. 2013;981:193–200.

Karr JW, Kaupp LJ, Szalai VA. Amyloid-beta binds Cu2+ in a mononuclear metal ion binding site. J Am Chem Soc. 2004;126(41):13534–8.

Landureau M, Redeker V, Bellande T, Eyquem S, Melki R. The differential solvent exposure of N-terminal residues provides "fingerprints" of alpha-synuclein fibrillar polymorphs. J Biol Chem. 2021;296:100737.

Lassen LB, Reimer L, Ferreira N, Betzer C, Jensen PH. Protein partners of α-synuclein in health and disease. Brain Pathol. 2016;26(3):389–97.

Lee H-J, Choi C, Lee S-J. Membrane-bound α-synuclein has a high aggregation propensity and the ability to seed the aggregation of the cytosolic form. J Biol Chem. 2002;277(1):671–8.

Lorentzon E, Horvath I, Kumar R, Rodrigues JI, Tamas MJ, Wittung-Stafshede P. Effects of the toxic metals arsenite and cadmium on alpha-synuclein aggregation in vitro and in cells. Int J Mol Sci. 2021;22(21):11455.

Lorentzon E, Kumar R, Horvath I, Wittung-Stafshede P. Differential effects of Cu(2+) and Fe(3+) ions on in vitro amyloid formation of biologically-relevant alpha-synuclein variants. Biometals. 2020;33(2):97–106.

Lovell MA, Robertson JD, Teesdale WJ, Campbell JL, Markesbery WR. Copper, iron and zinc in Alzheimer's disease senile plaques. J Neurol Sci. 1998;158(1):47–52.

Luk KC, Kehm V, Carroll J, Zhang B, O'Brien P, Trojanowski JQ, et al. Pathological alpha-synuclein transmission initiates Parkinson-like neurodegeneration in nontransgenic mice. Science. 2012;338(6109):949–53.

Manevich Y, Held KD, Biaglow JE. Coumarin-3-carboxylic acid as a detector for hydroxyl radicals generated chemically and by gamma radiation. Radiat Res. 1997;148(6):580–91.

Mason RJ, Paskins AR, Dalton CF, Smith DP. Copper binding and subsequent aggregation of alpha-synuclein are modulated by N-terminal acetylation and ablated by the H50Q missense mutation. Biochemistry. 2016;55(34):4737–41.

Masuda-Suzukake M, Nonaka T, Hosokawa M, Oikawa T, Arai T, Akiyama H, et al. Prion-like spreading of pathological alpha-synuclein in brain. Brain. 2013;136(Pt 4):1128–38.

Miller LM, Wang Q, Telivala TP, Smith RJ, Lanzirotti A, Miklossy J. Synchrotron-based infrared and X-ray imaging shows focalized accumulation of Cu and Zn co-localized with beta-amyloid deposits in Alzheimer's disease. J Struct Biol. 2006;155(1):30–7.

Miotto MC, Valiente-Gabioud AA, Rossetti G, Zweckstetter M, Carloni P, Selenko P, et al. Copper binding to the N-terminally acetylated, naturally occurring form of alpha-synuclein induces local helical folding. J Am Chem Soc. 2015;137(20):6444–7.

Miraglia F, Ricci A, Rota L, Colla E. Subcellular localization of alpha-synuclein aggregates and their interaction with membranes. Neural Regen Res. 2018;13(7):1136–44.

Moriarty GM, Minetti CA, Remeta DP, Baum J. A revised picture of the Cu(II)-alpha-synuclein complex: the role of N-terminal acetylation. Biochemistry. 2014;53(17):2815–7.

Öhrfelt A, Zetterberg H, Andersson K, Persson R, Secic D, Brinkmalm G, et al. Identification of novel α-synuclein isoforms in human brain tissue by using an online NanoLC-ESI-FTICR-MS method. Neurochem Res. 2011;36(11):2029–42.

Pedersen JT, Chen SW, Borg CB, Ness S, Bahl JM, Heegaard NH, et al. Amyloid-beta and alpha-synuclein decrease the level of metal-catalyzed reactive oxygen species by radical scavenging and redox silencing. J Am Chem Soc. 2016;138(12):3966–9.

Perni M, Galvagnion C, Maltsev A, Meisl G, Müller MBD, Challa PK, et al. A natural product inhibits the initiation of α-synuclein aggregation and suppresses its toxicity. Proc Natl Acad Sci. 2017;114(6):E1009–17.

Rasia RM, Bertoncini CW, Marsh D, Hoyer W, Cherny D, Zweckstetter M, et al. Structural characterization of copper(II) binding to alpha-synuclein: insights into the bioinorganic chemistry of Parkinson's disease. Proc Natl Acad Sci U S A. 2005;102(12):4294–9.

Recasens A, Dehay B, Bove J, Carballo-Carbajal I, Dovero S, Perez-Villalba A, et al. Lewy body extracts from Parkinson disease brains trigger alpha-synuclein pathology and neurodegeneration in mice and monkeys. Ann Neurol. 2014;75(3):351–62.

Rivillas-Acevedo L, Sanchez-Lopez C, Amero C, Quintanar L. Structural basis for the inhibition of truncated islet amyloid polypeptide aggregation by Cu(II): insights into the bioinorganic chemistry of type II diabetes. Inorg Chem. 2015;54(8):3788–96.

Sawaya MR, Hughes MP, Rodriguez JA, Riek R, Eisenberg DS. The expanding amyloid family: structure, stability, function, and pathogenesis. Cell. 2021;184(19):4857–73.

Smirnoff N. Ascorbic acid: metabolism and functions of a multi-facetted molecule. Curr Opin Plant Biol. 2000;3(3):229–35.

Spillantini MG, Schmidt ML, Lee VMY, Trojanowski JQ, Jakes R, Goedert M. α-Synuclein in Lewy bodies. Nature. 1997;388:839–40.

Teng X, Sheveleva A, Tuna F, Willison KR, Ying L. Acetylation rather than H50Q mutation impacts the kinetics of Cu(II) binding to alpha-synuclein. ChemPhysChem. 2021;22(23):2413–9.

Uversky VN. Neuropathology, biochemistry, and biophysics of α-synuclein aggregation. J Neurochem. 2007;103(1):17–37.

Uversky VN, Li J, Fink AL. Metal-triggered structural transformations, aggregation, and fibrillation of human alpha-synuclein. A possible molecular NK between Parkinson's disease and heavy metal exposure. J Biol Chem. 2001;276(47):44284–96.

Valiente-Gabioud AA, Torres-Monserrat V, Molina-Rubino L, Binolfi A, Griesinger C, Fernandez CO. Structural basis behind the interaction of Zn(2)(+) with the protein alpha-synuclein and the Abeta peptide: a comparative analysis. J Inorg Biochem. 2012;117:334–41.

Villar-Pique A, Lopes da Fonseca T, Sant'Anna R, Szego EM, Fonseca-Ornelas L, Pinho R, et al. Environmental and genetic

factors support the dissociation between alpha-synuclein aggregation and toxicity. Proc Natl Acad Sci U S A. 2016;113(42): E6506–15.

Wang C, Liu L, Zhang L, Peng Y, Zhou F. Redox reactions of the α-Synuclein−Cu2+ complex and their effects on neuronal cell viability. Biochemistry. 2010;49(37):8134–42.

Winner B, Jappelli R, Maji SK, Desplats PA, Boyer L, Aigner S, et al. In vivo demonstration that alpha-synuclein oligomers are toxic. Proc Natl Acad Sci U S A. 2011;108(10):4194–9.

Wittung-Stafshede P. Crossroads between copper ions and amyloid formation in Parkinson's disease. Essays Biochem. 2022;66(7): 977–86.

Zhang S, Li J, Xu Q, Xia W, Tao Y, Shi C, et al. Conformational dynamics of an alpha-synuclein fibril upon receptor binding revealed by insensitive nuclei enhanced by polarization transfer-based solid-state nuclear magnetic resonance and cryo-electron microscopy. J Am Chem Soc. 2023;145(8):4473–84.

SUPPORTING INFORMATION

Additional supporting information can be found online in the Supporting Information section at the end of this article.

How to cite this article: Walke G, Kumar R, Wittung-Stafshede P. Copper ion incorporation in α-synuclein amyloids. Protein Science. 2024;33(4): e4956. https://doi.org/10.1002/pro.4956